Chapter 4 Material Synthesis and Characterization

4.1 Introduction

The focus of this chapter is the synthesis and characterisation of materials intended to be employed as the photoelectrode layers in the dye-sensitized solar cells (DSSCs) that will be fabricated for this study. The most popular material for photoelectrodes in DSSCs is titanium dioxide (TiO_2) **[1]**. In addition to titanium dioxide, several materials were chosen for this study based on their HOMO and LUMO energy levels, including ZnO, CeO_2, CdS, CuO, and ZrO_2 **[2]**. The synthesis of TiO_2, a composite of TiO_2-ZrO_2, and a TiO_2-ZrO_2-Europium-doped composite are also included in this work as photoanode materials **[3-5]**.

The range of methods were employed to synthesize these materials, such as hydrothermal methods, the creation of alcogels or precipitates, or a combination of these methods. The materials' band gaps were ascertained by UV-Visible analysis using Tauc's plot, and they were characterized using X-ray diffraction (XRD). The samples' refractive index was determined using these band gap measurements.

4.2 Synthesis

ZnO

ZnO was prepared using the hydrothermal method **[6,7]**. Precursors $Zn(NO_3)_2{\cdot}6H_2O$ and NaOH, both of analytical grade, were utilized without further purification. Initially, 0.05 mol of NaOH and 0.005 mol of $Zn(NO_3)_2{\cdot}6H_2O$ were combined with 80 ml of distilled water, and the mixture was agitated using a magnetic stirrer until white precipitates started to form.. The precipitate was then poured into a 140-cc cylindrical stainless-steel autoclave lined with Teflon. After being sealed, the autoclave was heated for five hours at 180 °C in a furnace. Following the completion of the reaction and system cooling, the product was taken out and thoroughly washed with distilled water before being dried at 90 °C for five hours.

TiO_2

The hydrothermal method was employed to synthesis TiO_2 **[8,9]**. The precursors included HNO_3, isopropanol, and titanium isopropoxide. All of them were analytical quality, and they were used just as they were sent.

Solution A was first created by diluting 20 milliliters of titanium isopropoxide with 5 milliliters of isopropanol. To produce Solution B, combine 0.5 milliliters of water and 0.5 milliliters of HNO_3. Next, Solution B was gradually added to Solution A while being stirred using a room-temperature magnetic stirrer. After 30 minutes of stirring, an alcogel began to form. This alcogel was transferred to a stainless-steel autoclave and baked at 240°C for a full day. The precipitates that resulted from cooling were filtered and properly cleaned using isopropanol and distilled water, respectively.

CdS

The hydrothermal method was employed to prepare CdS **[10, 11]**, employing ethylene glycol, ethylene diamine, thiourea (NH_2CSNH_2), and cadmium chloride monohydrate ($CdCl_2 \cdot H_2O$) as precursors.

This method involved dissolving 0.01 mol of cadmium chloride and 0.03 mol of thiourea in 50 mL of ethylene glycol and ethylene diamine, respectively. These solutions were combined, and then they were placed in an autoclave that was 90% full.. After being sealed, the autoclave was heated for 12 hours at 180°C in an oven. Following the reaction, the yellow product was removed, cleaned in 100% ethanol, and let it dry in a nitrogen atmosphere at 100°C for five hours.

CeO_2

The hydrothermal method was employed to prepare CeO_2 **[12, 13]**. Sodium hydroxide (NaOH) and cerium nitrate hexahydrate ($Ce(NO_3)_2 \cdot 6H_2O$) were used as ingredients.

Initially, 0.217 grams of cerium nitrate hexahydrate and 0.280 grams of sodium hydroxide were dissolved in 5 millilitres and 35 millilitres of pure water, respectively. These solutions were mixed and stirred for 30 minutes at room temperature. After that, the mixture was poured in a Teflon-lined autoclave and maintained at a temperature of 180°C for 12 hours. Following the reaction, the autoclave was let to naturally cool down

to room temperature. After gathering the finished product, it was repeatedly cleansed with distilled water and ethanol. And then dried for six hours at 80°C.

For two hours, the dried sample was calcined again at 500°C. The process was repeated with an extended reaction period of 24 hours rather than 12 hours in order to obtain smaller CeO_2 particles.

ZrO_2

ZrO_2 was produced via the hydrothermal process **[14]**. The beginning materials were distilled water, isopropanol, zirconium propoxide, and HNO_3. Since they were all analytical quality, there was no need for additional filtration. Solution A was first made by diluting 20 millilitres of zirconium propoxide with 5 millilitres of isopropanol. 0.5 millilitres of distilled water and 0.5 millilitres of HNO_3 were combined to create Solution B. Next, Solution B was gradually added to Solution A while being stirred using a room-temperature magnetic stirrer. After 30 minutes of stirring, an alcogel began to form. Subsequently, the alcogel was heated for a whole day at 240°C in an oven and put in an autoclave. The precipitates were then filtered, carefully cleaned with distilled water, and finally treated with isopropanol.

CuO

Precipitation method was employed in the synthesis of CuO **[15]**. Cupric nitrate [$Cu(NO_3)_2$], sodium hydroxide [NaOH], and citric acid [$C_6H_8O_7$] were the first ingredients.

To make a 0.5 M solution of cupric nitrate, the chemical was first dissolved in 50 millilitres of distilled water and then stirred for 15 minutes. After that, sodium hydroxide solution was added to this mixture dropwise until the pH reached 12. After three hours of continuous swirling of the solution, a brown CuO precipitate developed. The precipitate was collected, thoroughly washed with ethanol and distilled water, and then dried to produce a powder. After that, the powder was heated to 450°C to anneal.

Undoped and Eu doped TiO_2-ZrO_2 nanocomposite

TiO_2-ZrO_2 (TZ) and Eu doped TiO_2-ZrO_2 (Eu doped TZ) nanocomposite were made by hydrothermal technique **[4]**. In 5 ml of isopropanol, Ti-isopropoxide and Zr-propoxide were diluted to generate a 70/30% molar ratio of TiO_2-ZrO_2. To achieve a 2 mol% doping of Eu in the TiO_2-ZrO_2 composite, Eu $(NO_3)_3$ was added to the solution mentioned above. After stirring the alkoxide solution at room temperature, 0.5 ml H_2O and 0.5 ml HNO_3 were added dropwise. Precipitates were prepared by transferring this solution into an autoclave lined with Teflon. The sample was maintained for 24 hours at 240°C at autogenic pressure. The sample was dried in a 100° C oven for two hours.

4.3. Characterization

The samples were characterized using X-ray diffraction (XRD). The band gap was discovered using UV-visible spectroscopy.

4.3.1 X-Ray Diffraction

The samples were subjected to room temperature X-ray powder diffraction using a Bruker D8 Advance X-ray Diffractometer. At room temperature, the 2θ range was measured in scan mode with a step increment of 0.05° and a step time of 2 seconds, spanning from 10° to 90°. Figures 1 through 6 show all of the samples' XRD patterns.

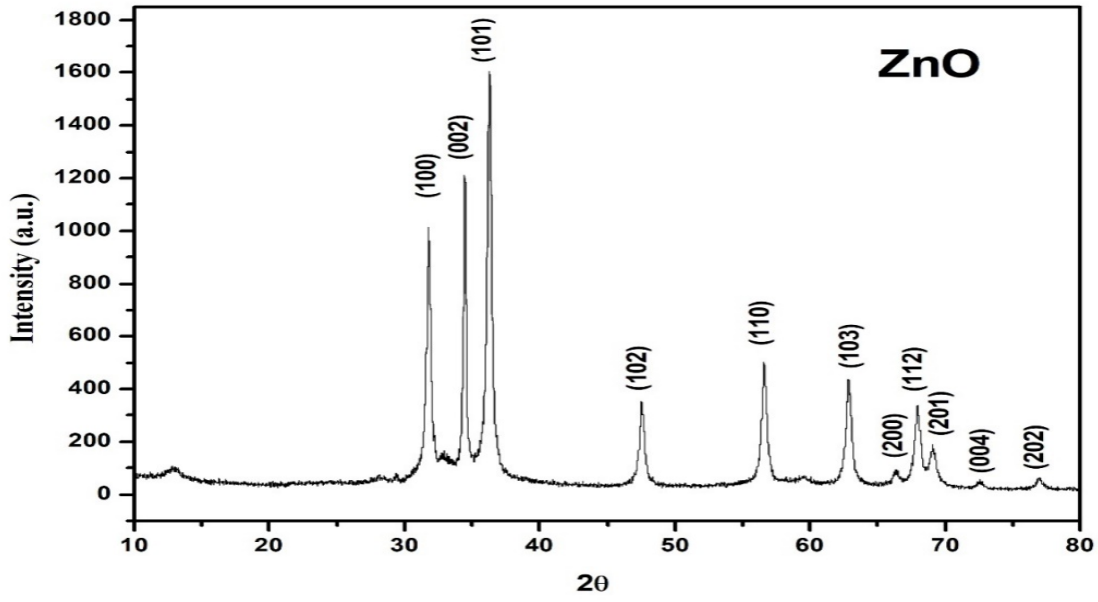

Figure 1: XRD pattern of ZnO.

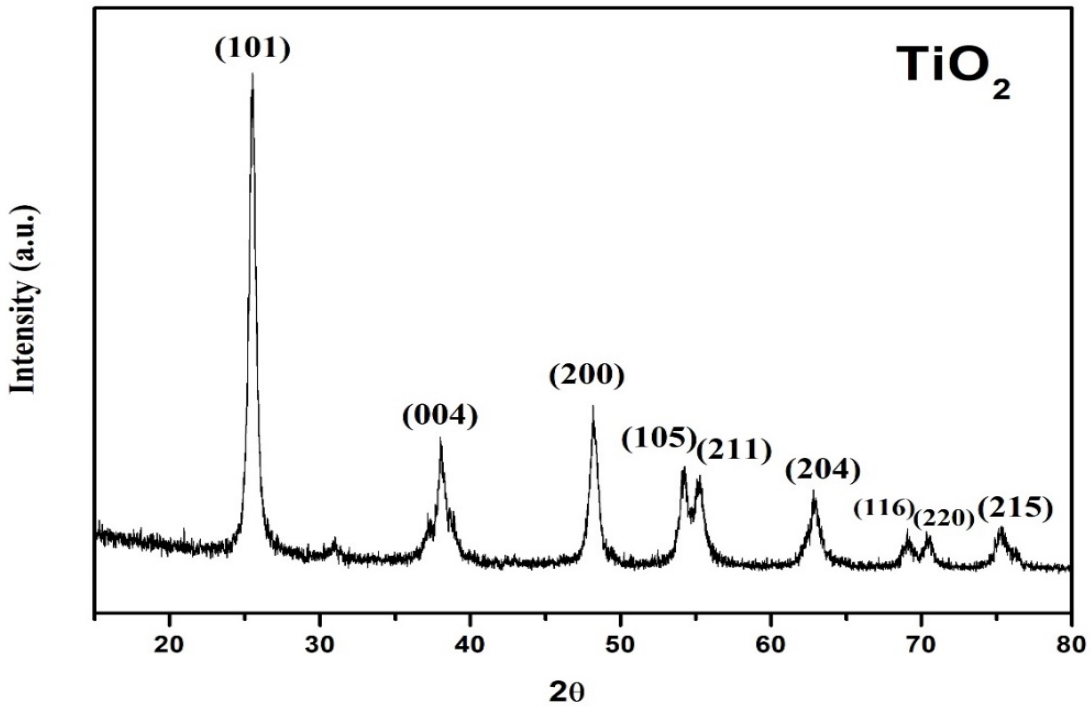

Figure 2: XRD pattern of TiO_2.

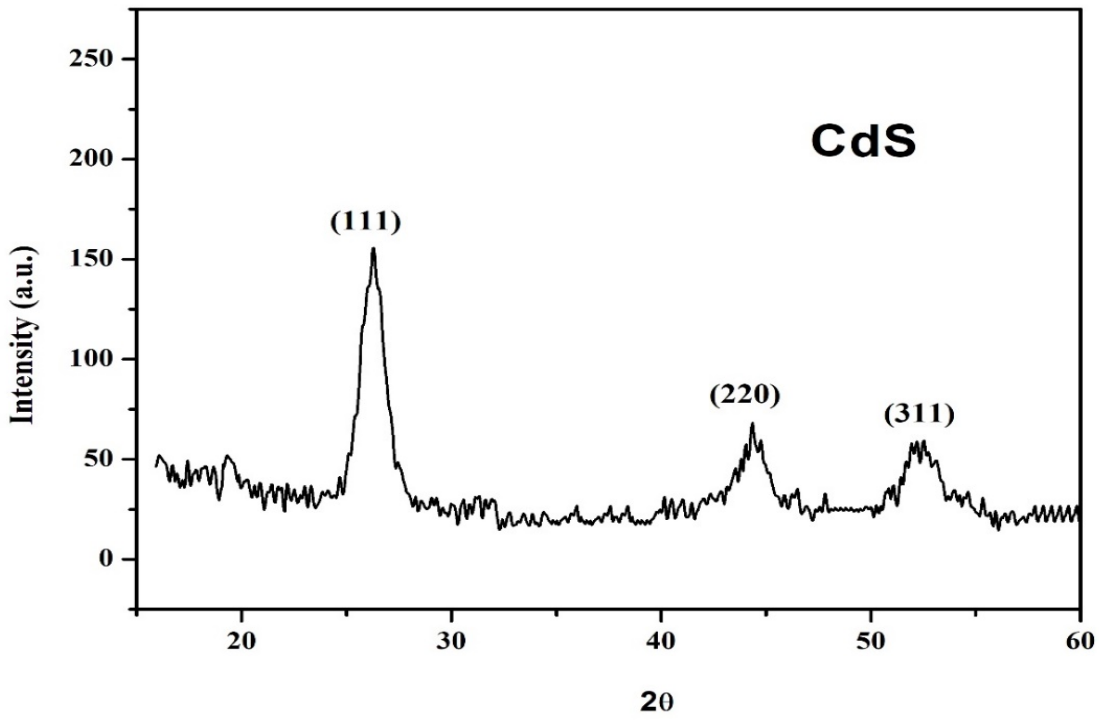

Figure 3: XRD pattern of CdS.

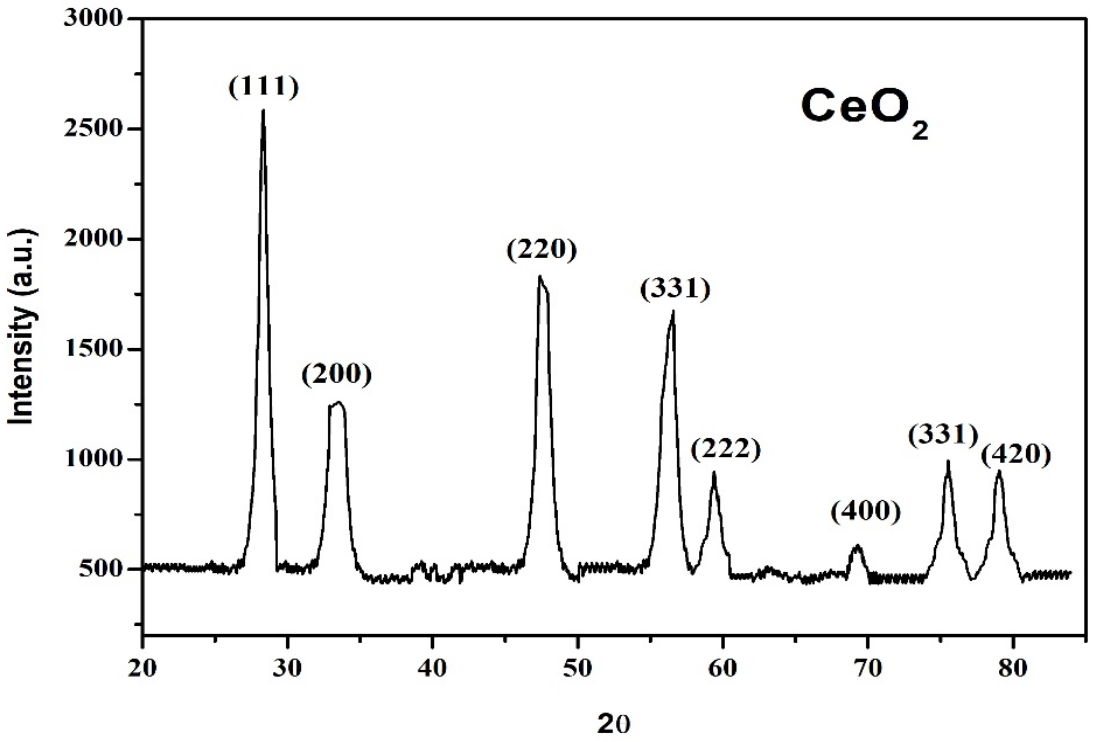

Figure 4: XRD pattern of CeO_2.

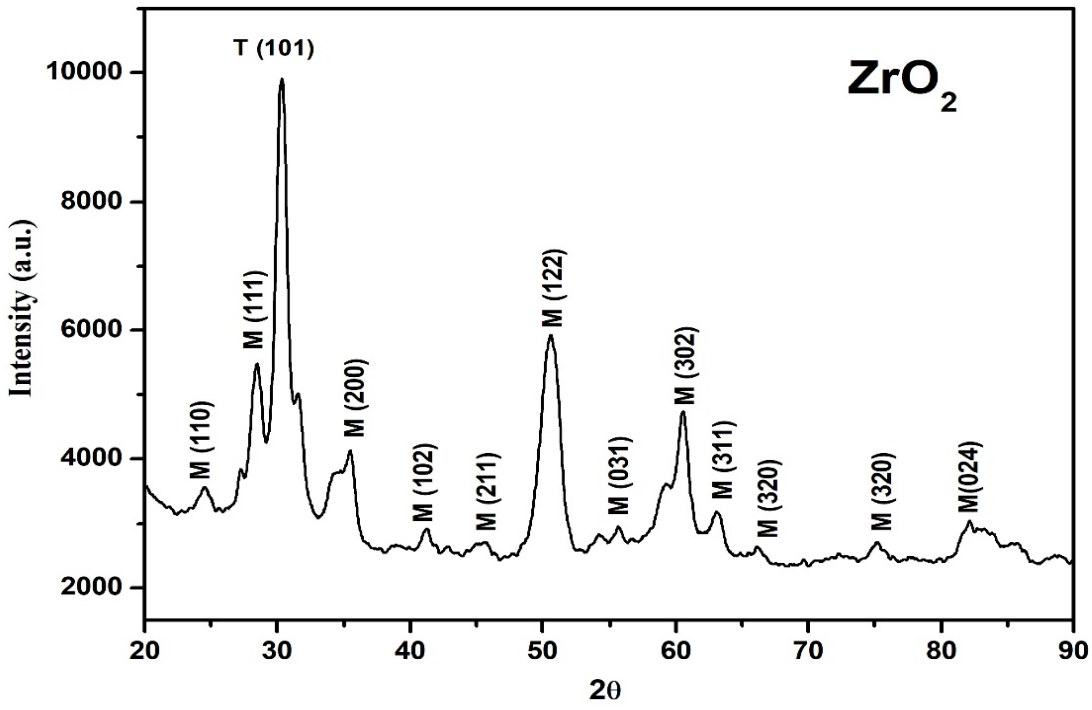

Figure 5: XRD pattern of ZrO_2.

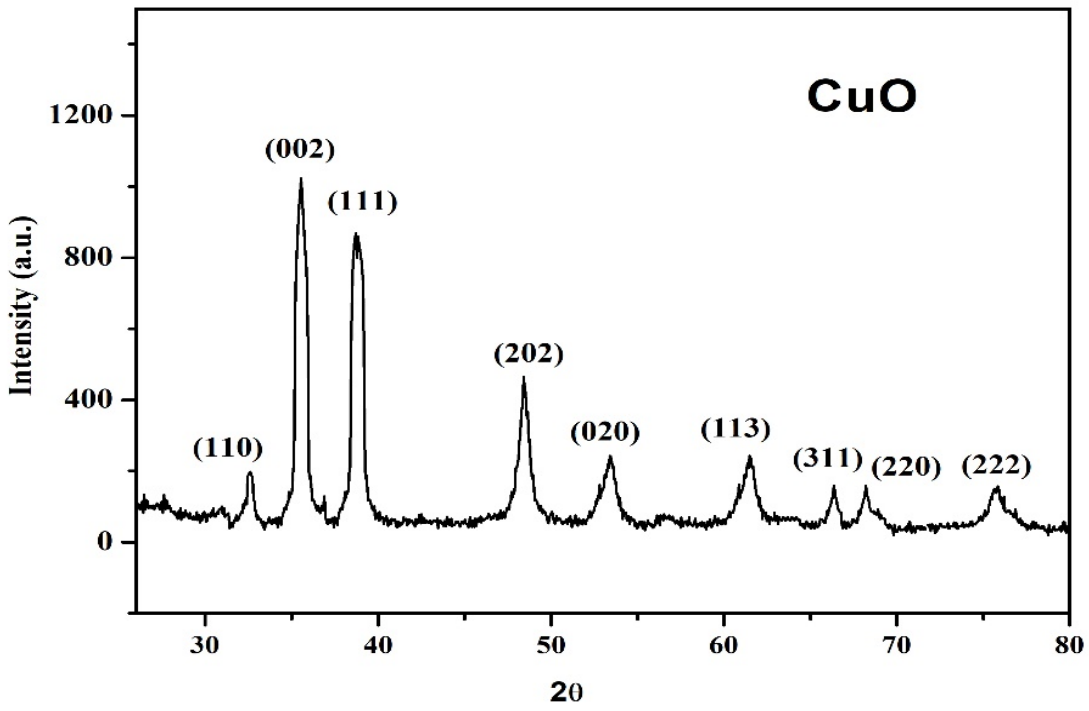

Figure 6: XRD pattern of CuO.

For most of the samples, the XRD peaks are bright and sharp. A high degree of crystallinity is indicated by the strong diffraction peaks.
A comparatively greater peak width is seen, suggesting the production of nanocrystalline material. The crystallite size was determined by Scherer formula.

Figure 1 displays the ZnO XRD patterns. The ZnO JCPDS (75-0576) and the diffraction measurements agreed well **[16]**. Each peak is distinct and strong. The average size of the crystallites was found to be 23.94 nm.

The TiO_2 XRD pattern is seen in Figure 2. The peaks are wide and pointed. The peaks' d values are extremely similar to those found in JCPDS file (21-1272) **[17]**. The peaks align with the anatase phase of TiO_2 peaks that are normally seen. With a 2θ value of 25.36°, the most powerful peak is the characteristic peak of the (101) plane. The size of a crystallite is 12.68 nm on average.

The CdS nanoparticles' XRD pattern is displayed in Figure 3. An example is the XRD of CdS, which displays just three peaks. These three prominent peaks, which measure 26.56°, 43.79°, and 52.85°, respectively, are indexed to the scattering from the

cubic CdS crystal lattice's (111), (220), and (311) planes. This matches the JCPDS card file number 75-1546 quite well **[18]**. A mean particle size of 20.82 nm was discovered.

Figure 4 displays the synthesized CeO_2 nanoparticles' XRD patterns. The JCPDS card number 34-0394 is used to index the peaks. Face centred Cubic shape is present in CeO_2 nanoparticles **[19]**. There are three main peaks: 28.56°, 47.47°, and 56.36°. It has been determined that the average crystallite size is 9.4 nm.

Figure 5 displays the ZrO_2 XRD pattern. ZrO_2 is present in both Monoclinic and Tetragonal phases, according to a match with the JCPDS database (Monoclinic ZrO_2-83-0944 and Tetragonal ZrO_2-79-1770) **[20]**. The average size of the crystallites was found to be 7.19 nm.

Figure 6 displays the CuO nanoparticles' XRD pattern. The peaks correspond to the monoclinic structure shown on JCPDS cards 89–5899 **[21]**. The average crystallite size was found to be 13.05 nm. No peaks other than the standard ones have been found in these patterns. It attests to the material's pure form development. ZrO_2 had the smallest average crystallite size, followed in order by CeO_2, TiO_2, CuO, CdS, and ZnO. Table 1 lists the average crystallite size of the samples.

Table 1: Structural Parameters of prepared samples.

Sample	Avg. Crystallite size	Crystallinity Index	JCPDS file no
ZnO	23.94 nm	93.06%	**75-0576**
TiO_2	12.68 nm	96.47%	21-1272
CdS	20.82 nm	85.89%	75-1546
CeO_2	9.4 nm	81.18%	34-0394
ZrO_2	7.19 nm	57.82%	83-0944 (Monoclinic) 79-1770 (Tetragonal)
CuO	13.05 nm	93.65%	89 - 5899

Composite samples

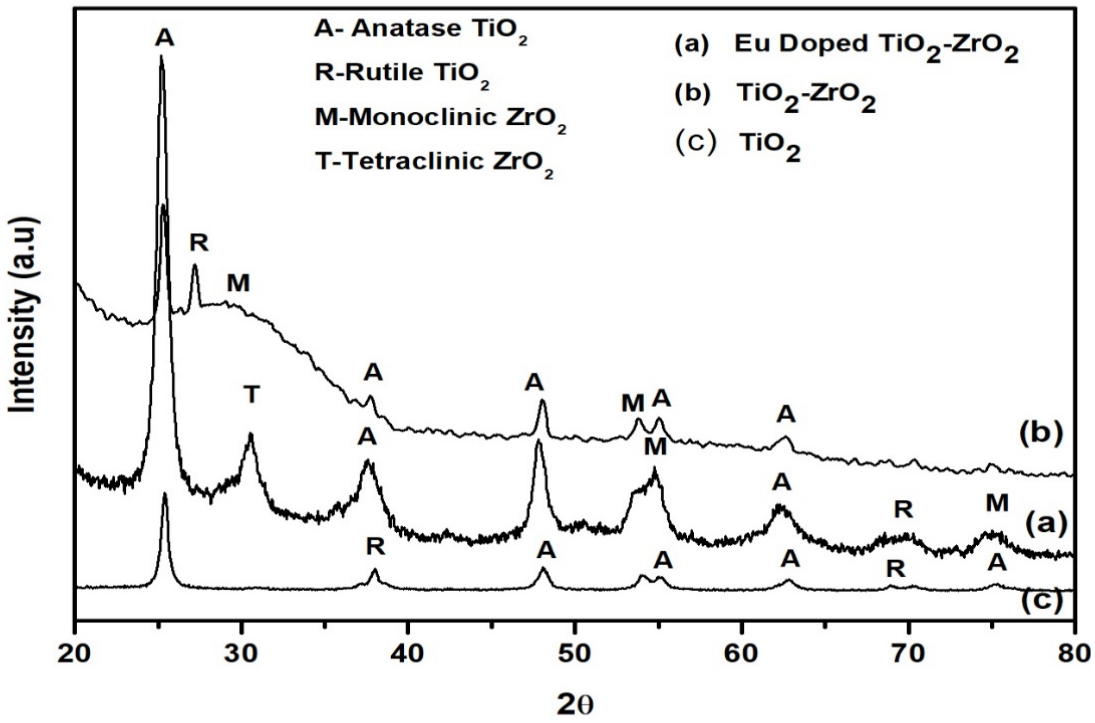

Figure 7: X-Ray Diffraction pattern of composite samples.

Figure 7 displays the composite samples' XRD pattern along with TiO_2. The JCPDS database [Anatase TiO_2 (21-1272), Rutile TiO_2 (21-1276), Monoclinic ZrO_2 (83-0944), and Tetragonal ZrO_2 (79-1770)] was used to identify the crystalline phase. ZrO_2 has been found in monoclinic and tetragonal phases, while TiO_2 has been identified in anatase and rutile phases. In every sample, the TiO_2 (101) Anatase peak is the most prominent characteristic. No other impurity peak has been discovered, indicating that the substance is found in its pure oxide form. The formula $f_A = [1 + 1.26(I_A/I_R)]^{-1}$ has been used to determine the mass fraction of anatase content. Here, 'f_A' stands for the mass fraction of anatase, 'I_A' for the intensity of the (101) peak of anatase, and 'I_R' for the intensity of the (110) peak of rutile. It was discovered that the anatase mass fraction in TiO_2, TiO_2-ZrO_2, and Eu doped TiO_2-ZrO_2 was, respectively, 79.60%, 48.71%, and 86.41%. The doping may be responsible for the stabilization of the anatase phase. An ideal stage for DSSC applications is anatase.

There is a considerable degree of crystallinity in the TiO_2 sample. When doped with Europium, the undoped TiO_2-ZrO_2 composite sample exhibits an improved degree of crystallinity. Consequently, it has been discovered that the doped sample's crystallinity

is superior to that of the undoped TiO_2-ZrO_2 sample. Thus, it seemed that the dopant was contributing to the samples' increased crystallinity.

Broad peaks indicate formation of material in nano size. The average crystallite size ($D = 0.9\lambda/\beta \cos\theta$, where 'β' denotes the whole width at half maximum of XRD lines) was determined using the Scherrer formula. TiO_2, TiO_2-ZrO_2, and Eu-doped TiO_2-ZrO_2 samples were found to have average crystallite sizes of 22.32 nm, 17.41 nm, and 6.47 nm, respectively. Particle size is reduced when ZrO_2 and TiO_2 are combined. Eu^{+3}, Zr^{+4}, and Ti^{+4} have ionic radii of 0.094, 0.072, and 0.069 nm, respectively. Eu's ionic radius is big. Therefore, it cannot take the place of the cation position in the TiO_2-ZrO_2 lattice; nevertheless, it can fit into the interstitial position, which may hinder the formation of crystals.

4.3.2. UV Visible Spectroscopy

A Thermo Fisher Scientific Evolution 600 Spectrophotometer was used to record the materials' UV-visible absorption spectra. Combinations of deuterium and tungsten halogen bulbs provide the light source.

Ethanol was used for dispersing the samples. After 30 minutes of sonication, the dispersion was moved to a quartz cuvette so that measurements could be taken. The scanning was conducted within a defined wavelength range of 200 nm to 900 nm. The samples' absorption spectra and Tauc's plots are displayed in figures 8 through 12. Table 2 presents the optical characteristics derived from UV-visible absorption spectra.

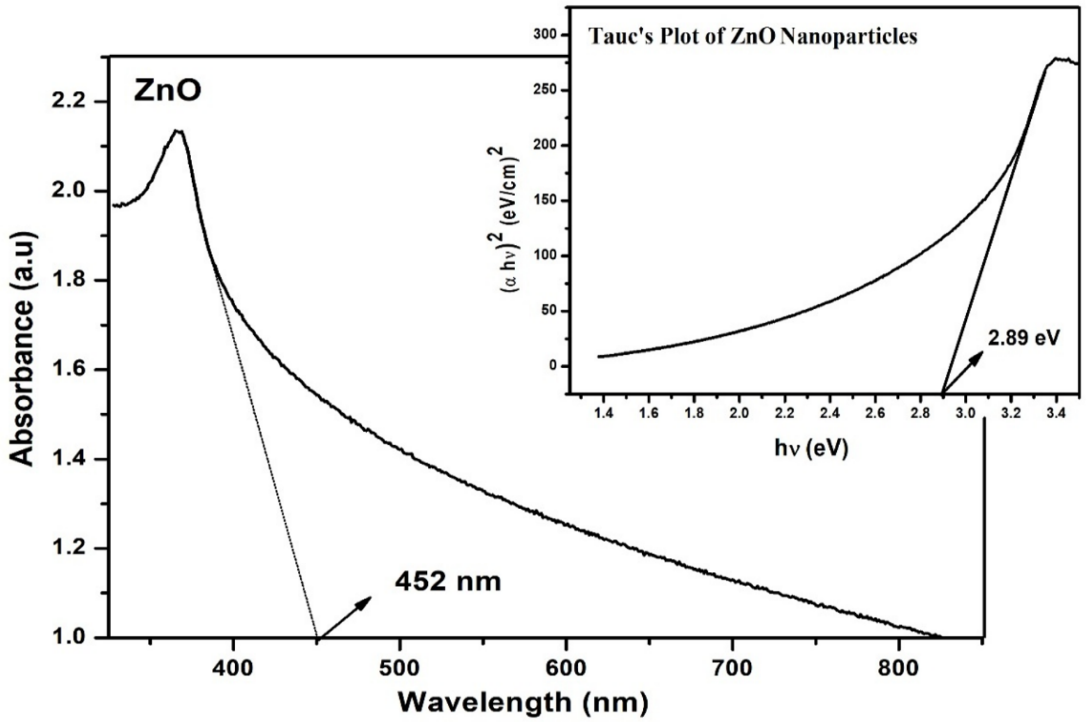

Figure 8: Absorption spectrum and Tauc's plot ZnO.

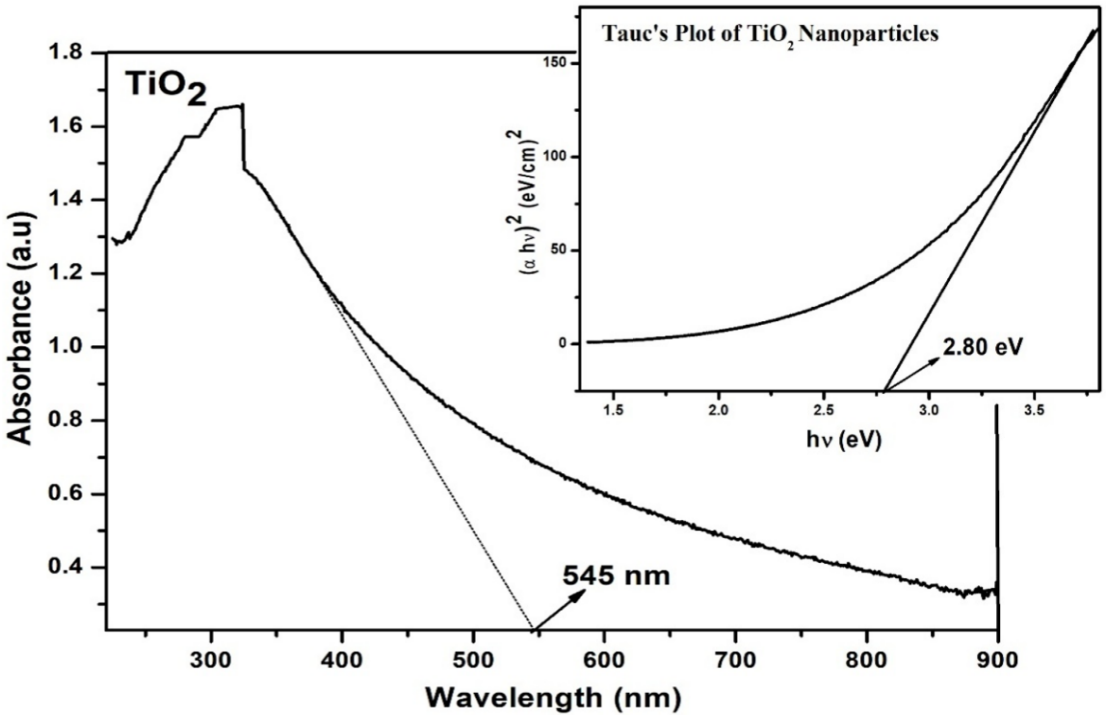

Figure 9: Absorption spectrum and Tauc's plot TiO_2.

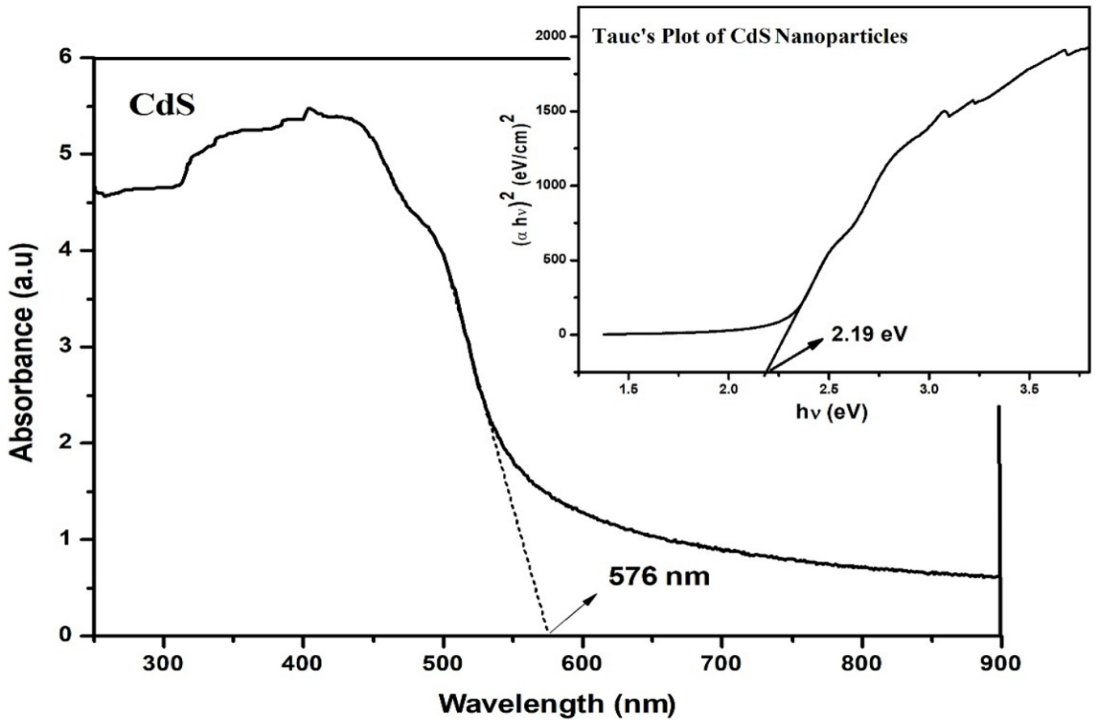

Figure 10: Absorption spectrum and Tauc's plot CdS.

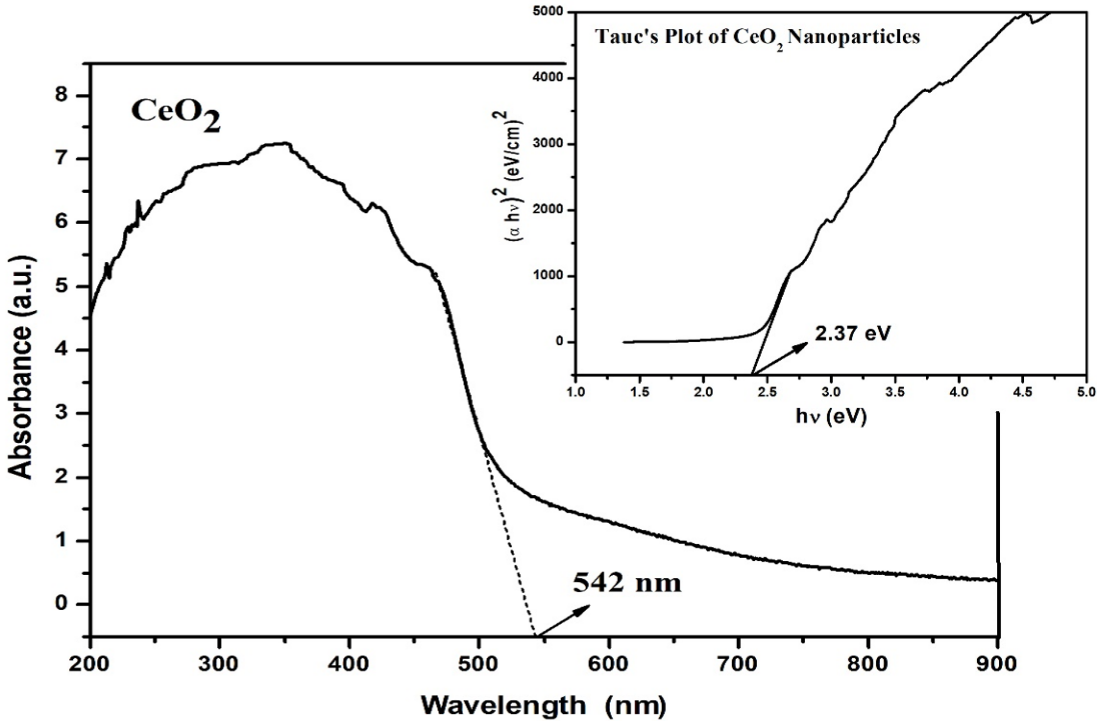

Figure 11: Absorption spectrum and Tauc's plot of CeO_2.

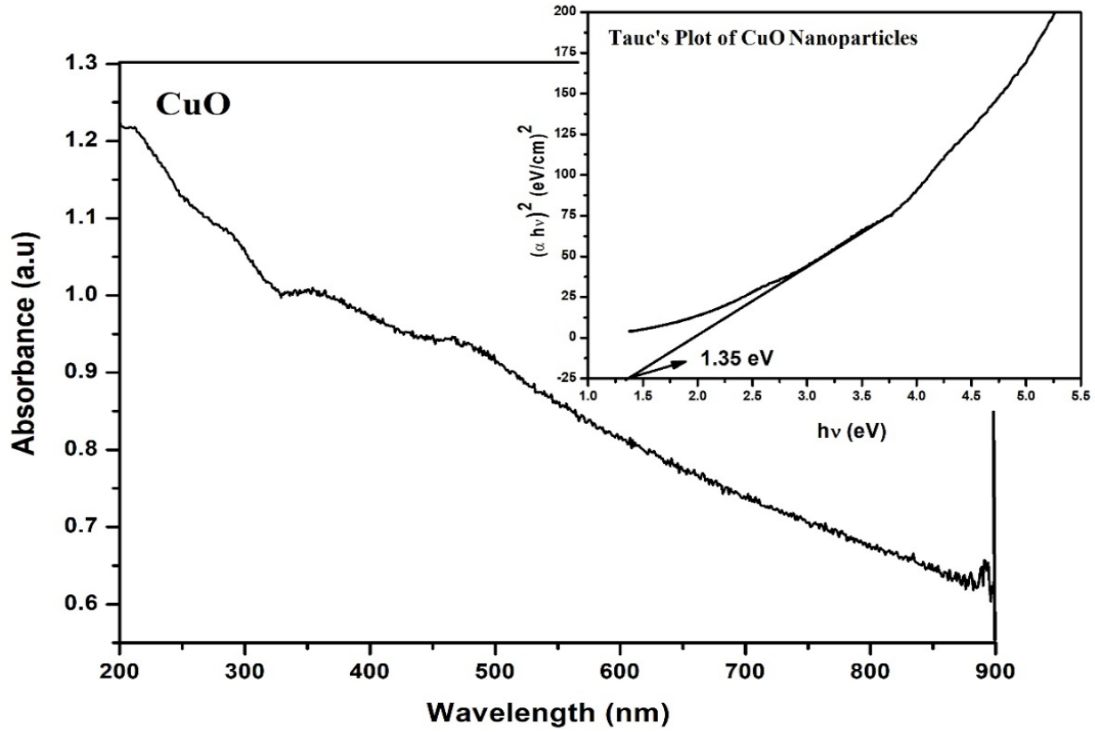

Figure 12: Absorption spectrum and Tauc's plot CuO.

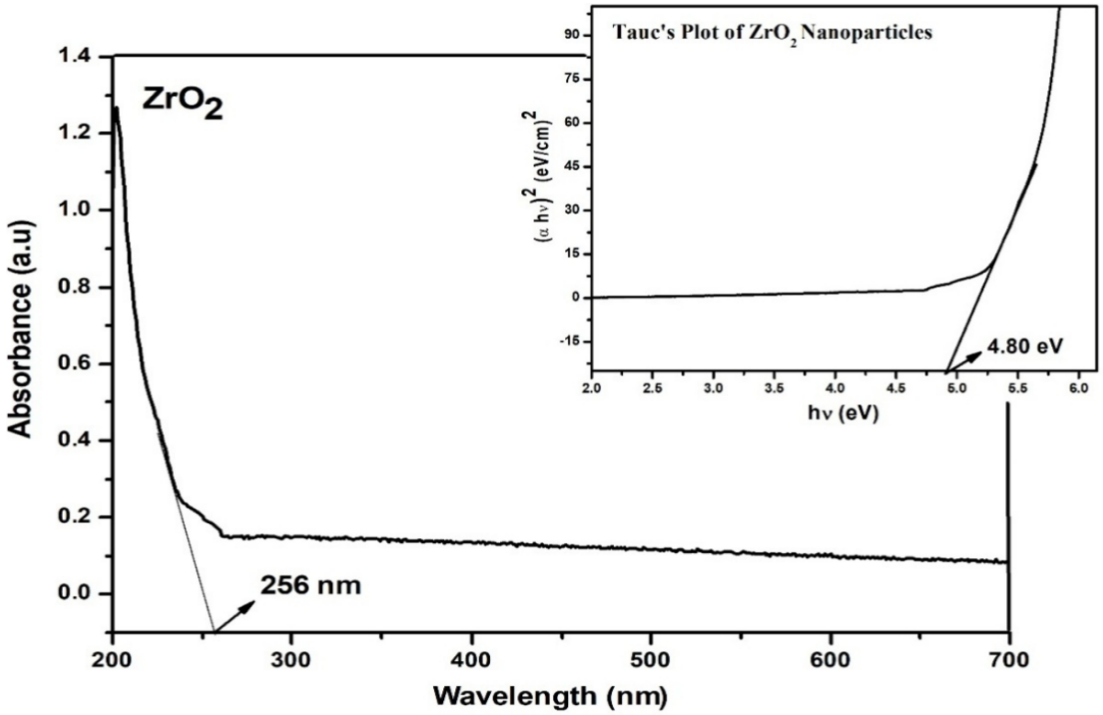

Figure 13: Absorption spectrum and Tauc's plot ZrO_2**.**

Table 2: Optical parameters of Prepared Materials.

Sample	Absorption Edge	Optical Bandgap (eV)	Absorption Co efficient (cm^{-1})	Extinction Co efficient	Refractive Index η	Optical Conductivity (Ω^{-1} cm^{-1})
ZnO	452 nm	2.89	3.72	1.27×10^{-5}	2.39	0.024
TiO_2	545 nm	2.80	2.19	7.72×10^{-6}	2.41	0.014
CdS	576 nm	2.19	3.60	1.62×10^{-5}	2.61	0.025
CeO_2	542 nm	2.30	4.54	1.87×10^{-5}	2.55	0.030
CuO	>900 nm	1.35	1.46	1.05×10^{-5}	3.04	0.012
ZrO_2	256 nm	4.80	0.39	8.12×10^{-7}	2.03	0.002

Table 2 lists all of the samples' absorption edges. All materials have demonstrated good absorption up to 600 nm, with the exception of ZrO_2. Below 260 nm, ZrO_2 exhibits absorption, suggesting a significant bandgap value. CuO exhibits broad absorption across the whole spectrum. This strong absorption across a large wavelength range may be advantageous for DSSC applications. The optical band gap, which was calculated using Tauc's figure, is also included in the Table. The optical band gap lies between 1.35 and 4.80 eV. CuO has the smallest band gap and ZrO_2 the largest. The samples range in refractive index from 2.03 to 3.04.

Composite samples

The absorption spectra of the composite samples are displayed in Figure 14. Samples of TiO_2-ZrO_2 and Eu-doped TiO_2-ZrO_2 exhibit a red shift in the absorption edge. The optical bandgap was calculated using Tauc's figure. Table 3 provides the calculated optical parameters. New energy levels below the conduction band may be introduced by the addition of Eu to TiO_2-ZrO_2. The reduced bandgap is the result of a decrease in the energy needed to transfer electrons from the valence band to the Eu^{+3} energy levels. Table 3 lists the optical bandgap and refractive index of the prepared samples. The table makes it evident that doping causes an increase in refractive index and a decrease in optical bandgap. The reduced bandgap is likely to prevent the recombination of photoelectrons with the oxidized electrolyte and dye. The new energy level that has been introduced below the conduction band because of metal doping boosts conductivity. More electrons

will be produced by the material's ability to retain incident light for a longer period due to its high refractive index and making it suitable for use in DSSC applications **[4]**.

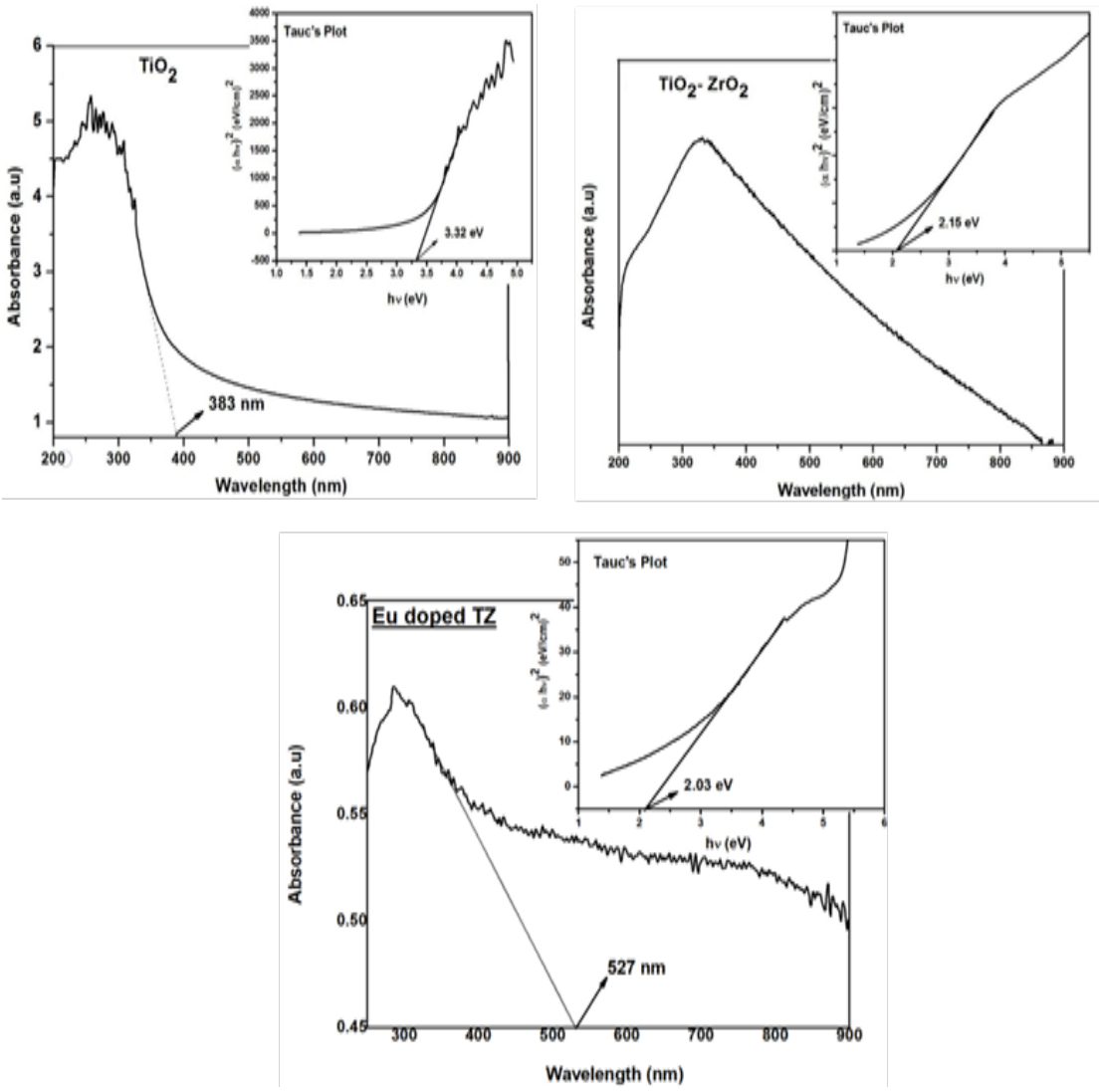

Figure 14: Absorption spectra of composite samples.

Table 3: Optical bandgap and refractive index of composite samples.

Sample	Optical Bandgap	Refractive Index
TiO_2	3.75 eV	2.21
TiO_2-ZrO_2	2.15 eV	2.63
Eu doped TiO_2-ZrO_2	2.03 eV	2.68

References:

1. Ahmad, M. S., Pandey, A. K., & Abd Rahim, N. (2017). Advancements in the development of TiO2 photoanodes and its fabrication methods for dye sensitized solar cell (DSSC) applications: A review. *Renewable and Sustainable Energy Reviews, 77*, 89-108.

2. Nuraje, N., Asmatulu, R., & Kudaibergenov, S. (2012). Metal oxide-based functional materials for solar energy conversion: A review. *Current Inorganic Chemistry (Discontinued), 2*(2), 124-146.
3. Tomar, L. J. (2017). Investigation of optical absorption, emission and photoelectric properties of rare earth and transition metal doped TiO2/ZrO2 compounds (Doctoral dissertation, Maharaja Sayajirao University of Baroda (India)).
4. Tomar, L., Bhatt, P., Desai, R., & Chakrabarty, B. (2022). Enhanced efficiency of dye sensitized solar cell using Eu doped TiO2-ZrO2 nanocomposite. *Recent Patents on Nanotechnology, 16*(4), 333-338.
5. Farheen, Fouad, H., Ansari, S. G., Khan, A. A., & Ansari, Z. A. (2017). Europium doped TiO2: An efficient photoanode material for dye sensitized solar cell. *Journal of Materials Science: Materials in Electronics, 28*, 6873-6879.
6. Pan, A., Yu, R., Xie, S., Zhang, Z., Jin, C., & Zou, B. (2005). ZnO flowers made up of thin nanosheets and their optical properties. *Journal of Crystal Growth, 282*(1-2), 165-172.
7. Xie, J., Wang, H., Duan, M., & Zhang, L. (2011). Synthesis and photocatalysis properties of ZnO structures with different morphologies via hydrothermal method. *Applied Surface Science, 257*(15), 6358-6363.
8. Tan, Z., Sato, K., & Ohara, S. (2015). Synthesis of layered nanostructured TiO2 by hydrothermal method. *Advanced Powder Technology, 26*(1), 296-302.
9. Vijayalakshmi, R., & Rajendran, V. (2012). Synthesis and characterization of nano-TiO2 via different methods. *Archives of Applied Science Research, 4*(2), 1183-1190.
10. Oliveira, J. F. A., Milao, T. M., Araujo, V. D., Moreira, M. L., Longo, E., & Bernardi, M. I. B. (2011). Influence of different solvents on the structural, optical and morphological properties of CdS nanoparticles. *Journal of Alloys and Compounds, 509*(24), 6880-6883.

11. Abd El-Sadek, M. S., Wasly, H. S., & Batoo, K. M. (2019). X-ray peak profile analysis and optical properties of CdS nanoparticles synthesized via the hydrothermal method. *Applied Physics A, 125*, 1-17.
12. Panahi-Kalamuei, M., Alizadeh, S., Mousavi-Kamazani, M., & Salavati-Niasari, M. (2015). Synthesis and characterization of CeO2 nanoparticles via hydrothermal route. *Journal of Industrial and Engineering Chemistry, 21*, 1301-1305.
13. Magdalane, C. M., Kaviyarasu, K., Siddhardha, B., & Ramalingam, G. (2021). Synthesis and characterization of CeO2 nanoparticles by hydrothermal method. *Materials Today: Proceedings, 36*, 130-132.
14. Sagadevan, S., Podder, J., & Das, I. (2016). Hydrothermal synthesis of zirconium oxide nanoparticles and its characterization. *Journal of Materials Science: Materials in Electronics, 27*, 5622-5627.
15. Phiwdang, K., Suphankij, S., Mekprasart, W., & Pecharapa, W. (2013). Synthesis of CuO nanoparticles by precipitation method using different precursors. *Energy Procedia, 34*, 740-745.
16. Chang, Y. C., Lin, Y. R., Chen, S. W., & Chou, C. M. (2022). Density-controlled growth of ZnO nanowalls for high-performance photocatalysts. *Materials, 15*(24), 9008.
17. Preethi, L. K., Mathews, T., Nand, M., Jha, S. N., Gopinath, C. S., & Dash, S. (2017). Band alignment and charge transfer pathway in three phase anatase-rutile-brookite TiO2 nanotubes: An efficient photocatalyst for water splitting. *Applied Catalysis B: Environmental, 218*, 9-19.
18. Oladeji, I. O., Chow, L., Liu, J. R., Chu, W. K., Bustamante, A. N. P., Fredricksen, C., & Schulte, A. F. (2000). Comparative study of CdS thin films deposited by single, continuous, and multiple dip chemical processes. *Thin Solid Films, 359*(2), 154-159.
19. Jayakumar, G., Irudayaraj, A. A., & Raj, A. D. (2017). Particle size effect on the properties of cerium oxide (CeO2) nanoparticles synthesized by hydrothermal method. *Mechanics, Materials Science & Engineering Journal, 9*(1).
20. Tomar, L. J. (2017). Investigation of optical absorption, emission and photoelectric properties of rare earth and transition metal doped TiO2/ZrO2 compounds (Doctoral dissertation, Maharaja Sayajirao University of Baroda (India)).

21. Jagadeesan, V., & Subramaniam, V. (2019). Impact of molarity on structural, optical, morphological and electrical properties of copper oxide thin films prepared by cost effective jet nebulizer spray pyrolysis technique. *Journal of Materials Science: Materials in Electronics, 30*, 1571-1578.